

# Asymmetric Effects Underlying Dynamic Heterogeneity in Miscible Blends of Poly(methyl methacrylate) with Poly(ethylene oxide)

Shannon Zhang and Michael A. Webb\*

*Department of Chemical and Biological Engineering, Princeton University, Princeton, NJ,  
08544 USA*

E-mail: mawebb@princeton.edu

## Abstract

The emergence of spatially variable local dynamics, or dynamic heterogeneity, is common in multicomponent polymer systems. Such heterogeneity is understood to arise from differences between the intrinsic dynamical fluctuations associated with one component versus another. However, the nature of the dynamic coupling between these components and how it depends on composition, temperature, and environmental fluctuations is not fully understood. Here, we use molecular dynamics simulations to characterize nanoscale dynamic heterogeneity in miscible blends of polyethylene oxide (PEO) and polymethyl methacrylate (PMMA) as a function of both temperature and blend composition. Probed over timescales of 100 ps, local PMMA segmental dynamics in blends align with neat PMMA when normalized by  $T_g$ , whereas PEO exhibits enhanced mobility caused by free-volume effects. The

effects of dynamical coupling are found to be asymmetric between the extent of enhancement to PMMA and suppression of PEO dynamics based on analysis of local environment composition within blends. Asymmetric effects in the melt state are also identified over longer timescales according to a Rouse mode analysis over larger sub-chains for each species. These results provide fundamental insights into how dynamic heterogeneity manifests at the nanoscale, across conditions and compositions in miscible polymer blends. They establish a foundation for exploring whether such asymmetries are generalizable and how dynamic heterogeneity can be tuned through temperature, composition, and morphology.

## 1 Introduction

Dynamic heterogeneity refers to spatial and temporal variations in the mobility and relaxation behavior of molecules or particles within a material. In polymer blends, such heterogeneity commonly arises due to differences in the intrinsic segmental dynamics of each component. When blended, interactions between polymers with distinct mobilities create coupled dynamical responses that manifest as perturbations across multiple spatiotemporal scales.<sup>1-6</sup> Consequently, the emergence of dynamic heterogeneity can strongly influence key material properties such as the glass transition temperature ( $T_g$ ),<sup>7-10</sup> viscoelastic behavior,<sup>11-15</sup> and ion conductivity.<sup>14,16-21</sup> Therefore, elucidating the molecular origins and characteristic length scales of dynamic heterogeneity is of fundamental scientific interest and may inform the design of polymer blends for targeted applications.

Dynamic heterogeneity is known to be significant in blends of polyethylene oxide (PEO) and polymethyl methacrylate (PMMA). While these polymers are miscible,<sup>22,23</sup> their glass transition temperatures ( $T_g$ ) differ by approximately 180 K.<sup>24,25</sup> This dissimilarity gives rise to pronounced differences in segmental dynamics when the polymers are blended, with relaxation times differing by up to 12 orders of magnitude.<sup>24,26</sup> Such contrast in mobilities has

implications for applications like solid polymer electrolytes,<sup>27–31</sup> where ionic conductivity is sensitive to local segmental fluctuations.<sup>32–34</sup> More broadly, PEO/PMMA blends serve as model systems for investigating dynamic coupling between components at the nanoscale, with signatures of heterogeneity accessible in both simulations and experiments.<sup>26,35–37</sup>

Numerous experimental studies have examined the dynamics of PEO and PMMA in blends under varying conditions. Quasi-elastic neutron scattering (QENS) on blends containing up to 30 wt% PEO has shown that the segmental mobility of PMMA, on length scales up to 11 Å, is primarily governed by the temperature difference between the system and the glass transition temperature of the blend, (i.e.,  $T - T_g$ ).<sup>38–40</sup> In contrast, PEO dynamics are strongly influenced by interactions with PMMA, exhibiting distinct behavior at short (<1 nm) and longer (>1nm) length scales.<sup>35,41</sup> At short length scales, QENS,<sup>36,42</sup> nuclear magnetic resonance (NMR),<sup>24,26</sup> and neutron spin echo (NSE) spectroscopy<sup>43</sup> reveal narrowing distributions of segmental relaxation times across a range of compositions and temperatures. These effects are attributed to self-concentration phenomena<sup>42</sup> and local confinement by the stiffer PMMA matrix, with a dependence on local free volume.<sup>24,26,36</sup>

On longer length scales, PEO dynamics have been investigated using infrared dichroism and birefringence,<sup>44</sup> QENS,<sup>36,41</sup> and NSE.<sup>35</sup> These measurements consistently indicate a pronounced slowdown of PEO segmental motion in blends with low PEO content.<sup>35,36,41,44</sup> Unlike the behavior observed at shorter scales, the dynamics at these larger scales are characterized by a broad distribution of relaxation times,<sup>36</sup> which is largely attributed to long-range concentration fluctuations.<sup>44</sup> Collectively, these observations highlight the presence of dynamic heterogeneity across multiple length scales in PEO/PMMA blends and suggest several underlying mechanisms; however, direct inference of the molecular-level phenomena remains elusive through experimental characterization alone.

To complement experimental observations, several theoretical models have been developed to explain dynamic heterogeneity in PEO/PMMA blends. The Lodge-McLeish

(LM) model, also referred to as the chain connectivity model, quantifies the influence of local self-concentration on polymer dynamics. The LM model predicts the segmental dynamics of each polymer component using the concentration within a cooperative volume centered on a monomer. The relevant length scale used to determine the size of the cooperative volume is the Kuhn length of each polymer component. It successfully predicts PEO relaxation times in blends containing 10-30 wt% PEO taken from QENS measurements for large spatial scales ( $q=0.69 \text{ \AA}^{-1}$ , approximately 18  $\text{\AA}$ ) but breaks down for smaller spatial scales ( $q=1.3 \text{ \AA}^{-1}$ , approximately 10  $\text{\AA}$ ).<sup>36</sup> When the self-concentration is allowed to vary as a fitting parameter, the LM model reasonably fits PEO relaxation times measured by QENS<sup>36</sup> and NMR,<sup>26</sup> as well as terminal PMMA relaxation times.<sup>45</sup> However, allowing the self-concentration to vary obfuscates the theoretical foundations of and insights from the model.

Another model uses mesoscale concentration fluctuations with length scales between 1 nm and 1  $\mu\text{m}$  via the generalized entropy theory of glass formation, the lattice cluster theory of blend thermodynamics, and the Kirkwood-Buff theory of concentration fluctuations to predict structural relaxation times of dynamically asymmetric miscible polymers in blends.<sup>46,47</sup> It can qualitatively fit the separated relaxation times of PEO and PMMA in blends but cannot account for the chemical specificity required for fitting quantitative behaviors.<sup>46,47</sup>

Finally, a coupling model<sup>48-52</sup> and the generalized Langevin equation framework<sup>53-55</sup> have been developed to describe a crossover time that separates single-chain PEO dynamics at short length scales from many-chain coupled PEO dynamics at long length scales. This framework has been used to explain unexpected phenomena and properties that arise specifically in dynamically asymmetric miscible polymer blends, such as different  $T_g$  values for each component and the breakdown of the time-temperature superposition.<sup>50</sup> Additionally, the coupling model closely captures PEO segmental dynamics for experimental QENS

measurements using a momentum transfer  $q$  value between 1 and 2  $\text{\AA}^{-1}$  in blends with 10-30 wt% PEO.<sup>36</sup> These theories qualitatively capture and rationalize trends in blended PEO dynamics up to mesoscale length scales. However, like with experimental observations, they do not conclusively illustrate the molecular-level phenomena that contribute to dynamic heterogeneity.

Molecular dynamics (MD) simulations have helped to elucidate the microscopic origins of dynamic heterogeneity in polymer blends under certain conditions. Analysis of all-atom simulations with blend compositions of 10-30 wt% PEO suggest the presence of multiple populations of PEO dynamics in blends which may be caused by confinement effects of PEO in a rigid matrix of PMMA. This is deduced from van Hove self-correlation functions of hydrogen atoms from PEO, which show a double-peak structure at 400 K with an unmoving second peak<sup>41</sup> and PEO relaxation times that are broadly distributed.<sup>56</sup> Monitoring mean-square deviations of atoms in PEO and PMMA also suggests highly disparate local cage sizes, as the magnitude of distance traveled in the ballistic regime is much higher for PEO than PMMA.<sup>41,56</sup> Additionally, PEO segmental relaxation times have been found to be more stretched upon blending than those of PMMA.<sup>56</sup> Rouse analyses based on simulations of 20 wt% PEO have illustrated the non-Gaussianity of the distribution of PEO atomic displacements in blends<sup>57</sup>, suggesting that local PEO segmental motion for wavelengths on the order of the size of a monomer is not strongly affected by blending but is more strongly affected at larger wavelengths.<sup>37</sup> These results provide molecular-level insights into dynamic heterogeneity in PEO/PMMA blends, albeit using a varied set of compositions, temperatures, and characterization methods.

In this work, we use atomistic MD simulations to systematically characterize how dynamic heterogeneity manifests at the nanoscale in PEO/PMMA blends. A central objective is to examine how the strength of dynamic coupling between the two components depends on temperature and blend composition. Although prior studies have explored the dynamic

behavior of PEO/PMMA blends, inconsistencies in system specifications (e.g., blend composition, molecular weight, and force field) as well as differences in thermodynamic conditions have made it difficult to identify clear trends. To address this, we comprehensively investigate behavior over a full range of blend compositions and at temperatures above, between, and below the simulated apparent  $T_g$  of both polymers. Dynamics are characterized by means of both local segmental fluctuations as well as segmental relaxation timescales. We find that blending induces asymmetric and composition-dependent changes in both local and collective dynamics, governed by temperature, local composition, and local structure. These findings help to clarify what PEO-PMMA interactions influence dynamic heterogeneity and motivate further investigation into their generality and implications for macroscopic properties and functional performance.

## 2 Methods

### 2.1 Simulation

#### 2.1.1 General simulation protocols

All MD simulations are performed using LAMMPS (ver 29, Sep 2021).<sup>58</sup> Systems are modeled using the all-atom optimized potentials for liquid simulations (OPLS-AA)<sup>59</sup> force field. Real-space non-bonded interactions are truncated at 12 Å. Long-range electrostatics are handled using the particle-particle-particle-mesh Ewald summation method with a  $10^{-4}$  convergence accuracy.<sup>60,61</sup> Equations of motion are integrated using a velocity-Verlet integration scheme and a 1 fs timestep. Periodic boundary conditions are used in all three dimensions. Temperature and pressure are controlled using a Nosé-Hoover thermostat and barostat with damping constants of 100 fs and 2000 fs, respectively.

### 2.1.2 Polymer chain generation

Each PEO chain consists of 75 monomers, and each PMMA chain consists of 33 monomers. As a result, chains for both polymers possess molecular weights of approximately 33,000 g/mol. Initial chain configurations are generated to match the expected average squared end-to-end distance,  $\langle R^2 \rangle = Ll_k$ , where  $L$  is the contour length and  $l_k$  is the Kuhn length of the polymer. The contour length  $L$  is estimated from the fully extended conformation of each polymer using geometry optimization in Avogadro 1.2.0 with the steepest descent algorithm and the UFF force field;<sup>62,63</sup> this yields values of 326.1 Å for PEO and 102.5 Å for PMMA. The Kuhn lengths used are 8.2 Å for PEO and 13.8 Å for PMMA.<sup>64</sup> Chains are constructed by sequentially adding monomers, with each new monomer positioned based on a randomly sampled dihedral angle. For PEO, dihedral angles are drawn from a uniform distribution between  $-0.65$  and  $0.65$  radians; for PMMA, the range is  $-0.4$  to  $0.4$  radians. For each system described below, this process is repeated until the required number of independent chain configurations within a threshold of 5 Å of the target  $\langle R^2 \rangle$  is obtained. These configurations are used as described in Section 2.1.3.

### 2.1.3 System preparation

Systems are specified in terms of their composition, given by the fraction of PEO chains relative to all chains in the simulation cell. We use the notation

$$x^{(\text{PEO})} \equiv \frac{N^{(\text{PEO})}}{N^{(\text{PEO})} + N^{(\text{PMMA})}} \quad (1)$$

where  $N^{(\text{PEO})}$  and  $N^{(\text{PMMA})}$  are the number of chains of PEO and PMMA. Because the PEO and PMMA chains possess similar molecular weights,  $x^{(\text{PEO})}$  is also comparable to the mass fraction of PEO in the system. Condensed-phase systems are then prepared for  $x^{(\text{PEO})} = 0, 0.1, 0.2, 0.3, 0.4, 0.5, 0.6, 0.7, 0.8, 0.9,$  and  $1.0$ . Each system contains

$N^{(\text{PEO})} + N^{(\text{PMMA})} = 40$  total chains. For each  $x^{(\text{PEO})}$ , three independent systems are prepared, resulting in a total of  $11 \times 3 = 33$  systems.

For each system, an initial configuration is generated by randomly placing each pre-constructed chain into a  $60 \text{ \AA} \times 60 \text{ \AA} \times 60 \text{ \AA}$  simulation box with random positions and orientations. A brief energy minimization is then performed where the system is simulated in the microcanonical (NVE) ensemble with a constrained maximum distance of  $0.005 \text{ \AA}$  moved per timestep; this minimization takes place for  $0.05 \text{ ns}$ . After, the constrained maximum distance is increased to  $0.1 \text{ \AA}$  and the system is simulated for  $0.5 \text{ ns}$ . This procedure resolves unfavorable atomic overlaps introduced by the random packing procedure. Following minimization, initial velocities for all particles are randomly generated with a uniform distribution at  $300 \text{ K}$ . The system undergoes  $1 \text{ ns}$  of simulation in the NVE ensemble, followed by  $1 \text{ ns}$  in the canonical (NVT) ensemble at  $300 \text{ K}$ . Subsequently, a barostat is introduced to maintain the pressure at  $1 \text{ atm}$ , and the system is heated from  $300 \text{ K}$  to  $700 \text{ K}$  at a rate of  $80 \text{ K/ns}$ . After reaching  $700 \text{ K}$ , the system is equilibrated in the isothermal-isobaric (NPT) ensemble for  $50 \text{ ns}$ . Finally, the system is cooled from  $700 \text{ K}$  to  $100 \text{ K}$  at a rate of  $10 \text{ K/ns}$  at constant pressure.

The cooling trajectories are used for analysis of glass transition temperatures (see Section 2.2.1). Simulation configurations are also recorded specifically around the temperatures of  $500 \text{ K}$ ,  $360 \text{ K}$ , and  $220 \text{ K}$ . From these configurations, additional simulations are performed for  $35 \text{ ns}$  in the NPT ensemble. These simulation trajectories are used to characterize dynamic heterogeneity by means of local segmental mobilities, as described in Sections 2.2.2 and 2.2.3. Finally, systems at  $500 \text{ K}$  and all compositions except  $x^{(\text{PEO})} = 0.0$ , and systems at  $360 \text{ K}$  and  $x^{(\text{PEO})} = 0.6$  to  $1.0$ , are simulated for an additional  $100 \text{ ns}$  to enable the Rouse mode analysis described in Section 2.2.4. For  $x^{(\text{PEO})} = 0.0$  at  $500 \text{ K}$ , the simulation is extended by  $200 \text{ ns}$  to improve statistical sampling.

We note that our system preparation protocol yields amorphous systems across all com-

positions and temperatures. As such, the following analysis pertains to well-mixed systems without the influence of crystallization, which is not accessible on simulation timescales. While semicrystallinity is an important factor for material properties, its absence here removes a potential confounding factor, allowing a clearer focus on the fundamental dynamical coupling between components.

## 2.2 Analysis

### 2.2.1 Glass transition temperature

To obtain an apparent glass transition temperature ( $T_g$ ), we use simulated dilatometry and analyze the temperature dependence of the specific volume,  $v(T)$ , for each system. An apparent  $T_g$  is identified by a change in the slope of  $v(T)$ ,<sup>65,66</sup> which reflects a shift in thermophysical relaxation behavior for the monitored quantity; this is associated with transition from a melt to a more glassy state. During the cooling phase of system preparation (Section 2.1.3), configurations are recorded at 10 K intervals. For each temperature, we perform an additional 1 ns simulation under isothermal–isobaric (NPT) conditions, starting from the corresponding configuration. The average specific volume is computed from the second half of each trajectory, yielding a set of  $(T_i, \bar{v}_i)$  pairs.

The apparent  $T_g$  from this dataset is determined using a previously reported bootstrap resampling procedure.<sup>20,21</sup> We first identify, by visual inspection, a maximum and minimum temperature within the melt regime,  $T_{\max}^m$  and  $T_{\min}^m$ , and a maximum and minimum temperature within the glassy regime,  $T_{\max}^g$  and  $T_{\min}^g$ . The temperatures  $T_{\min}^m$  and  $T_{\max}^g$  define sampling ranges for the melt,  $[T_{\min}^m, T_{\max}^m = T_{\min}^m + 100 \text{ K}]$ , and for the glass,  $[T_{\min}^g = T_{\max}^g - 100 \text{ K}, T_{\max}^g]$ . The temperature bounds used for each blend composition are listed in the Supplementary Information, Table S1. In each resampling iteration, a lower bound  $T_{\text{lo}}^m$  is randomly selected from the melt range and an upper bound  $T_{\text{hi}}^g$  from the glass

range. Linear regressions are then performed on the data within  $[T_{\text{lo}}^{\text{m}}, T_{\text{max}}^{\text{m}}]$  and  $[T_{\text{min}}^{\text{g}}, T_{\text{hi}}^{\text{g}}]$  to fit the melt and glassy branches, respectively. The intersection of these fits defines a  $T_{\text{g}}$  sample. This process is repeated 10,000 times to generate a distribution of  $T_{\text{g}}$  values. We report the mean of this distribution as the estimated  $T_{\text{g}}$  and its standard deviation as the associated uncertainty. Simulated  $v(T)$  data and representative  $T_{\text{g}}$  values for each blend composition are provided in the Supplementary Information, Figure S1.

### 2.2.2 Local segmental mobility

To characterize local segmental dynamics, we define a segmental mobility parameter,  $\mu_{i,\Delta t}$ , which relates to the mean-square fluctuation of the positions of a particle over a given observation time  $\Delta t$ . For a given particle  $i$ , a mobility is computed as

$$\mu_{i,\Delta t} = \frac{\langle (\vec{r}_i(t) - \langle \vec{r}_i \rangle_{\Delta t})^2 \rangle_{\Delta t}}{\Delta t} \quad (2)$$

where  $i$  is a backbone carbon,  $\vec{r}_i(t)$  is the position of particle  $i$  at time  $t$ , and  $\langle \cdot \rangle_{\Delta t}$  denotes an ensemble average over the observation time. For the analysis herein,  $\Delta t = 100$  ps, which is substantially shorter than timescales for chain diffusion. Consequently, eq. (2) mostly captures local segmental fluctuations. This quantity is computed at 500 K, 360 K, and 220 K from the final 5 ns of the 35-nanosecond trajectories described in Section 2.1.3. Analysis based on  $\mu_{i,\Delta t}$  across compositions and temperatures manifests in two ways. In Section 3.2, the segmental mobility is computed at the species level by averaging over all backbone carbons of each polymer type. In Section 3.3, the segmental mobility is further resolved based on the local environment of each backbone carbon atom to account for compositional heterogeneity introduced by blending.

To characterize the local environment of a particle, we define a normalized self-density parameter,  $\tilde{\phi}_i^{(A)}$ , which measures the local enrichment of species  $A$  around a particle of the

same species. For a given backbone carbon atom  $i$ , this quantity is computed as:

$$\tilde{\phi}_i^{(A)} = \frac{\sum_{j=1}^n \omega_{ij}^{(A)} \delta_{\alpha_j}^{(A)}}{\langle \sum_{j=1}^n \omega_{ij}^{(A)} \rangle_{x^{(A)}=1}} \quad (3)$$

In eq. (3), the numerator sums over all  $n$  monomers in the system, applying position-dependent weights  $\omega_{ij}^{(A)}$  and selecting only those monomers of species  $A$  via the Kronecker delta  $\delta_{\alpha_j}^{(A)}$ , where  $\alpha_j$  denotes the species identity of monomer  $j$ . The denominator provides a normalization by the average local density around a particle in a pure  $A$  system (subjected to the same weighting coefficients), denoted by  $\langle \cdot \rangle_{x^{(A)}=1}$ . This normalization provides natural limits then of  $\tilde{\phi}_i^{(A)} = 1$  corresponding to a local environment identical to that in a pure system of species  $A$ , while  $\tilde{\phi}_i^{(A)} = 0$  indicates a local environment composed entirely of the other species.

To utilize eq. (3), a scheme for the weighting coefficients must be defined, of which there are many reasonable choices. We choose to define a smoothing kernel of the form

$$\omega_{ij}^{(A)} = \begin{cases} 1 & r_{ij} \leq \mu^{(A)} \\ \exp\left(-\frac{(r_{ij} - r_m^{(A)})^2}{\sigma^2}\right) & r_{ij} > \mu^{(A)} \end{cases} \quad (4)$$

where  $r_{ij} = |\vec{r}_i - \vec{R}_j|$  is the distance between particle  $i$  and the center of mass of monomer  $j$  (using the minimum image convention), and  $r_m^{(A)}$  and  $\sigma$  are parameters that define a smoothing kernel. To emphasize spatially local interactions, we set  $r_m^{(A)}$  to the radius of gyration of a single monomer of species  $A$ , computed from simulations in vacuum at room temperature. This yields  $r_m^{(\text{PEO})} = 1.59 \text{ \AA}$  and  $r_m^{(\text{PMMA})} = 2.34 \text{ \AA}$ . The smoothing width parameter is set to  $\sigma = 12 \text{ \AA}$  based on the non-bonded, real-space interaction cutoff.

### 2.2.3 Free-volume analysis

The concept of free volume is often invoked to elucidate facets of polymer dynamics.<sup>67–70</sup> To quantify the free volume associated with each polymer chain, we implement the following procedure. First, the simulation cell is tessellated using Delaunay triangulation, such that each simplex (tetrahedron) is defined by four atoms. Each chain is associated with a subset of simplices that have at least one vertex belonging to an atom on that chain. Next, the entire simulation cell is filled with a three-dimensional grid of  $n$  equally spaced spherical probes, where  $n$  depends on a chosen probe radius. Each probe is then classified as occupied or unoccupied based on overlap with any atom in the system, using atomic diameters defined by the  $\sigma$  parameters from the OPLS-AA force field. Finally, the free volume of a given chain is then computed as the total volume of unoccupied probes that fall within the chain-associated simplices. Free volume is computed and averaged over the final 5 ns of simulations equilibrated at 500 K, 360 K, and 220 K. In the main text, results correspond to a probe radius of 0.5 Å; additional results for other probe sizes are provided in Figure S2.

### 2.2.4 Rouse mode analysis

To investigate how dynamic heterogeneity manifests in collective polymer dynamics, we perform a Rouse mode analysis to extract characteristic relaxation times associated with different statistical segment lengths of the polymer chains. For a polymer comprised of  $N$  monomers, Rouse mode coordinates are computed by

$$\vec{X}_p(t) = \sqrt{\frac{c_p}{2}} \sum_{i=0}^{N-1} \vec{r}_i(t) \cos \left[ \frac{p\pi}{N} \left( i + \frac{1}{2} \right) \right] \quad (5)$$

where  $p = 0, \dots, N - 1$  indicates the mode index,  $\vec{r}_i(t)$  is the position of the center of mass of the  $i$ th monomer on the chain at time  $t$ , and  $c_p$  is a  $p$ -dependent constant, such

that  $c_1 = 1$  and  $c_p = 2$  for all other modes. The zeroth mode corresponds to the behavior of the center of mass of a chain, while all other modes roughly correspond to the collective behavior of sub-chains of  $\frac{(N-1)}{p}$  segments.

The Rouse mode coordinates are used to compute time autocorrelation functions (ACFs), which characterize the relaxation timescales of subchains of varying segment lengths. Each ACF is well-described by a stretched exponential function:

$$\frac{\langle \vec{X}_p(t) \cdot \vec{X}_p(0) \rangle}{\langle \vec{X}_p(0) \cdot \vec{X}_p(0) \rangle} = \exp \left[ - \left( \frac{t}{\tau_p} \right)^{\beta_p} \right] \quad (6)$$

where  $\tau_p$  and  $\beta_p$  are fitting parameters. Rather than fitting ACFs to eq. (6), however, ACFs are fit to a linearized form of eq. (6) for simplicity. Taking the natural logarithm yields

$$\ln \left[ - \ln \left( \frac{\langle \vec{X}_p(t) \cdot \vec{X}_p(0) \rangle}{\langle \vec{X}_p(0) \cdot \vec{X}_p(0) \rangle} \right) \right] = \beta_p \ln(t) - \beta_p \ln(\tau_p) \quad (7)$$

allowing extraction of  $\beta_p$  and  $\tau_p$  via linear regression. An effective relaxation time is then calculated as

$$\tau_p^{\text{eff}} = \int_0^\infty \exp \left[ - \left( \frac{t}{\tau_p} \right)^{\beta_p} \right] dt = \tau_p^{1/\beta_p} \Gamma \left( \frac{\beta_p + 1}{\beta_p} \right) \quad (8)$$

where  $\Gamma(\cdot)$  denotes the gamma function. To perform the fitting, the ACF is computed over 8000 ps for PMMA and over 2000 ps for all other systems. These time intervals ensure that, at the highest temperature 500 K, the average normalized ACF of the largest  $p$  mode of each species in each system reaches at least 0.5. For reference, representative ACFs and fitted curves are provided in the Supplementary Information, Figures S4 and S5.

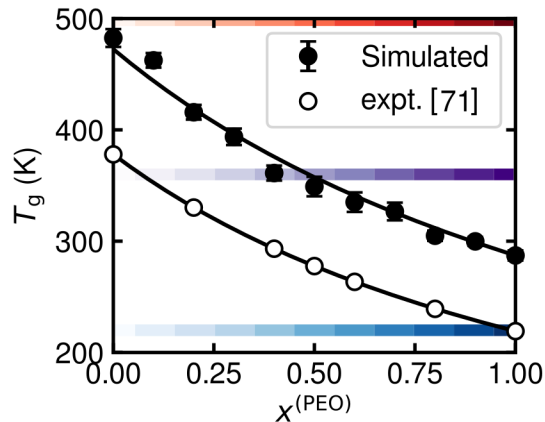


Figure 1: Dependence of glass transition temperature ( $T_g$ ) on blend composition. Markers represent simulated (filled) and experimental (empty)  $T_g$  values for blends of PEO and PMMA. Experimental results are from Ref. 71. Solid black lines are fits to the Fox equation. Error bars reflect standard errors calculated from three independent system configurations. Horizontal, colored bands provide visual reference to 500 K (red), 360 K (purple), and 220 K (blue), which are examined in subsequent figures. The color gradation within each band distinguishes blends at the same temperature but different compositions.

### 3 Results & Discussion

#### 3.1 Composition-dependent glass transition temperatures

We begin by briefly comparing experimental and simulated trends regarding  $T_g$  for these PEO/PMMA systems as a function of composition. Figure 1 shows that both the simulated apparent  $T_g$  as well as the experimental  $T_g$  values<sup>71</sup> follow the Fox equation

$$\frac{1}{T_g} = \frac{w^{(\text{PEO})}}{T_g^{(\text{PEO})}} + \frac{w^{(\text{PMMA})}}{T_g^{(\text{PMMA})}} \quad (9)$$

where  $w^{(i)}$  is the mass fraction of species  $i$  and  $T_g^{(i)}$  is the  $T_g$  of a pure neat system of species  $i$ . The apparent  $T_g$  values extracted from simulation are systematically higher than experimental values by approximately 100 K. This offset is roughly consistent across the range of examined compositions and is generally expected due to the much faster cooling

rates and shorter observation times inherent to molecular simulations.<sup>72,73</sup> Given this systematic disparity, the similarity in trends and alignment with the Fox equation suggests that the employed force field captures the essential physics governing blend dynamics and responds appropriately to changes in composition.

Figure 1 also highlights three temperatures that are of specific interest in the following sections. These temperatures are selected to span distinct dynamical regimes: (i) 220 K lies below the apparent  $T_g$  of both pure components and therefore below that of any blend; (ii) 360 K falls between the  $T_g$  values of pure PEO and PMMA, such that some blends are above and others below their respective  $T_g$ ; and (iii) 500 K exceeds the  $T_g$  of both pure components and all blends. This temperature range enables the examination of how interspecies dynamical coupling depends not only on the different  $T_g$  values of PEO and PMMA but also on the absolute temperature with respect to these  $T_g$  values.

### 3.2 Characterization of species-dependent local dynamics

As an initial characterization of nanoscale dynamic heterogeneity, we examine how blending influences the average local dynamics of PEO and PMMA compared to their behavior in neat systems. Specifically, we analyze species-resolved segmental mobilities ( $\mu_{i,\Delta t}$ ) of polymer segments across varying blend compositions at temperatures below (220 K), between (360 K), and above (500 K) the apparent  $T_g$  values of the pure components.

Figures 2A and 2B show the  $\mu_{i,\Delta t}$  as a function of  $T - T_g$ , where  $T_g$  varies with composition. The dynamics for PEO in blends (Figure 2A) exhibit significant deviations from neat behavior at the same distance from  $T_g$  (dashed black line) across most compositions but particularly in PMMA-rich blends (low  $x^{(\text{PEO})}$ ). This indicates that  $T - T_g$  is not a reliable predictor of local segmental dynamics for PEO. In contrast, PMMA (Figure 2B) dynamics in blends closely follow the behavior of neat PMMA, albeit with less strong correlation at temperatures below  $T_g$ . This trend is consistent with previous findings suggesting that

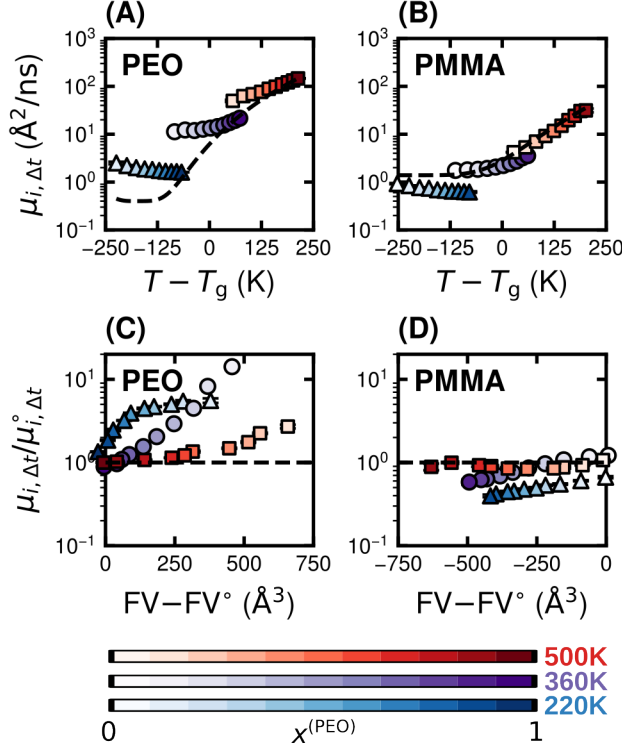


Figure 2: Analysis of local segmental mobilities across blend compositions and temperatures. The local segmental mobility,  $\mu_{i,\Delta t}$  as a function of temperature relative to the apparent  $T_g$  for (A) PEO and (B) PMMA. The dashed black lines represent fits to the neat polymer reference,  $\mu_{i,\Delta t}^\circ$ . Segmental mobility as a function of free volume (FV) for (C) PEO and (D) PMMA. The  $FV^\circ$  denotes reference to the FV of the neat polymer. Error bars reflecting standard errors from three independent systems are generally smaller than the symbol size.

PMMA dynamics are effectively governed by the temperature difference from the  $T_g$  of the blend<sup>38–40</sup> and also reveal an asymmetry in dynamical coupling between PEO and PMMA.

To elucidate the prior results, we examine variations in species-dependent packing behavior, which is expected to manifest in different free volumes of the chains. Figures 2C and 2D show the normalized segmental mobility as a function of a change in free volume from the neat system (denoted by ‘ $\circ$ ’). The rationale for this comparison derives from considerations involving free-volume theory, which may suggest that  $\log[\mu_{i,\Delta t}/\mu_{i,\Delta t}^\circ] \propto (FV - FV^\circ)$ . The data indeed possess roughly linear in the limit of smaller perturbations in FV. The positive trends in Figures 2C and 2D across all temperatures indicate that positive devi-

ations in segmental mobility from neat polymer behavior generally correlate with increases in local free volume upon blending and vice versa. One exception is the dynamics of PMMA at high temperature, which is largely insensitive to changes in FV. Both PEO and PMMA chains in blends with lower  $x^{(\text{PEO})}$  exhibit greater free volume. We attribute this to less effective packing of PMMA relative to PEO due to sterics from the acrylate functional group. These trends support the notion that packing effects contribute to dynamic heterogeneity, but they again highlight an asymmetry in coupling. While increased free volume tends to correlate with enhanced mobility for PEO, a reduction in free volume does not universally imply suppressed segmental dynamics in PMMA by the same magnitude. This asymmetry reflects the influence of other factors beyond free volume in controlling relative enhancement/suppression of polymer dynamics in blends.

### 3.3 Influence of local environment on segmental mobility

While previous results focused on local dynamics at the species level, we now explicitly consider variations due to the local environment of individual polymer segments. The central hypothesis is that a PEO segment surrounded entirely by other PEO segments should behave similarly to one in a pure PEO system, with minimal influence from PMMA, and vice versa. However, as the local environment becomes enriched in the opposite species, there will be interaction-based coupling that will lead to deviations. To test this, we analyze segmental mobilities as a function of a normalized self-density parameter  $\tilde{\phi}_i^{(A)}$ , which is approximately unity when the environment is similar to that of the neat system and approaches zero when surrounded completely by the other species.

Figure 3 shows that the influence of local environment is asymmetric between species and strongly temperature-dependent. In cases where  $\mu_{i,\Delta t}$  is enhanced upon blending (above the dashed line),  $\mu_{i,\Delta t}$  gradually approaches the neat reference,  $\mu_{i,\Delta t}^\circ$ , as the local environment becomes enriched in the same species; the notion of gradual in this context re-

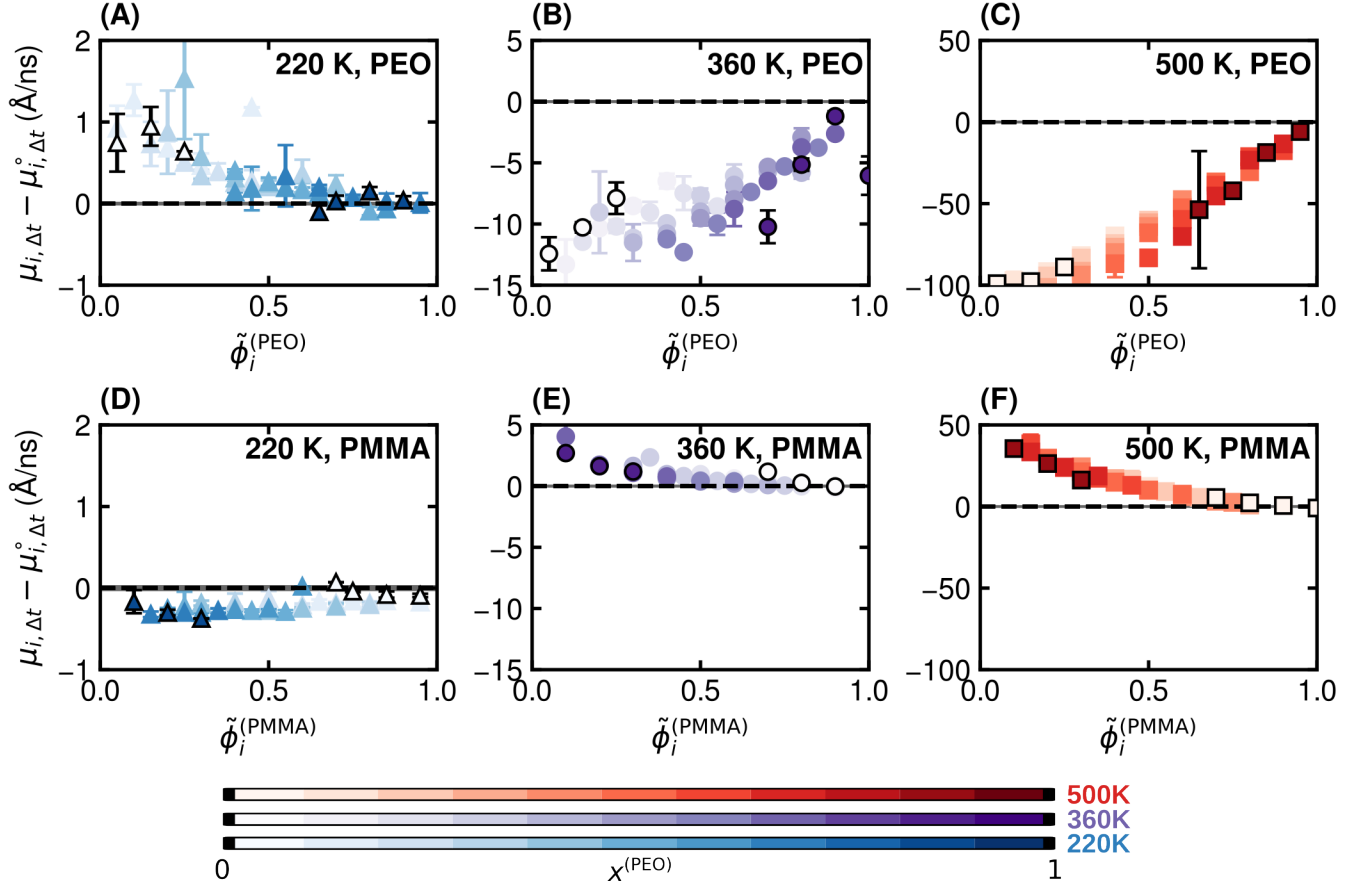


Figure 3: Variation in relative segmental mobility based on local environment. Deviations for neat-polymer mobility for PEO at (A) 220 K, (B) 360 K, and (C) 500 K and for PMMA at (D) 220 K, (E) 360 K, and (F) 500 K. Data is shown for all blend compositions, with gradation from light (PMMA-rich) to dark (PEO-rich), as indicated by the color bars. Results for chains in blends with the most extreme compositions ( $x^{(\text{PEO})} = 0.1$  and  $0.9$ ) are outlined in black for visual clarity. Error bars reflect standard errors from three independent systems. Horizontal dashed lines provide a guide to the eye for the neat-polymer mobility. The gray shaded area around the dashed lines reflect standard deviations calculated from three independent neat systems.

flects a vanishing of the first derivative,  $\frac{\partial \mu_{i,\Delta t}}{\partial \phi_i}$ . Where  $\mu_{i,\Delta t}$  is suppressed (below the dashed line),  $\mu_{i,\Delta t}$  approaches  $\mu_{i,\Delta t}^0$  more abruptly. While all dynamics tend to the neat reference in the limit of that the local environment is enriched in that species, these behaviors, which are species-agnostic, reveal that suppression effects are more readily evident than enhancements. In other words, the local coupling of polymers with the opposing species

has a much stronger magnitude of effect of reducing the mobility of faster-moving chains than enhancing the mobility of slower-moving chains in a blend. Upon investigation of the behavior of  $\mu_{i,\Delta t} - \mu_{i,\Delta t}^\circ$  normalized by  $\mu_{i,\Delta t}^\circ$  shown in Figure S3, it is evident, however, that the relative change in  $\mu_{i,\Delta t}$  is actually much larger for species with enhanced mobility than suppressed mobility.

There is also disparity in the composition-dependence of these observations between the two polymer species. In PEO, Figures 3B and 3C show that trends in segmental mobility with respect to  $\tilde{\phi}_i^{(\text{PEO})}$  differ based on  $x^{(\text{PEO})}$ . We observe that the extent of dynamical coupling is weaker in blends with more PMMA (i.e., for a given  $\tilde{\phi}_i^{(\text{PEO})}$ ,  $\mu_{i,\Delta t} - \mu_{i,\Delta t}^\circ$  is smaller in systems with lower  $x^{(\text{PEO})}$ ). By contrast, in PMMA, Figures 3E and 3F show how  $\mu_{i,\Delta t} - \mu_{i,\Delta t}^\circ$  collapses onto a single curve for all compositions. This can be accounted for by the composition-dependent packing behavior. Namely, the suppression of PEO mobility due to the presence of more PMMA in the local environment is negated in part by the larger free volume, which would tend to enhance mobility of chains in PMMA-rich blends (Figure 2). This effect is largely absent for PMMA at all temperatures, once again reflecting the asymmetrical nature of dynamic heterogeneity in these blends.

### 3.4 Rouse mode analysis of collective dynamics in the melt state

To gain insight into how blending affects the length scale of altered collective dynamics of PEO and PMMA, we perform a Rouse mode analysis on chains of both species. The departure from local dynamics to collective dynamics allows us to probe longer time and length scale behaviors in the blends. This analysis is limited to systems where all species remain in the melt state, both given the computational challenges of equilibration and statistical convergence as well as the dramatic increase in relaxation times expected at temperatures below the  $T_g$  of PEO or PMMA. Results are shown at the highest temperature of 500 K in Figure 4 and at 360 K in the Supplementary Information, Figure S6.

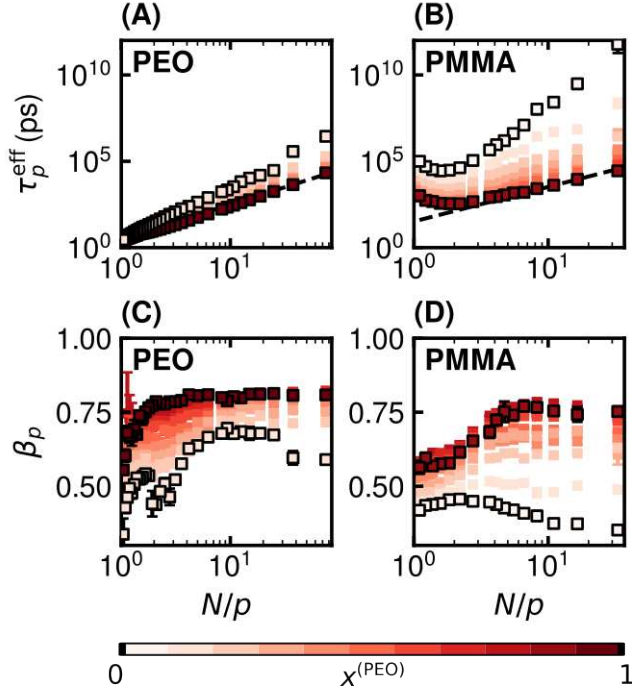


Figure 4: Rouse mode analysis at 500 K for chains in blends of varying composition. The effective Rouse relaxation time  $\tau_p^{\text{eff}}$  as a function of sub-chain length  $N/p$  for (A) PEO and (B) PMMA. The mode-dependent stretching exponent  $\beta_p$  for (C) PEO and (D) PMMA. For  $p > 8$ , symbols for data are only shown for every third value of  $p$  for visual clarity. Dashed black lines in panels (A) and (B) are a guide to the eye to indicate the expected ideal scaling of  $\tau_p \sim p^{-2}$ . The position of the line is the same across panels and is set to align with the behavior of neat PEO. Results for chains in blends with the most extreme compositions are outlined in black for visual clarity of trends. Error bars reflect standard errors from three independent systems and are generally smaller than the symbol size.

Figure 4A shows that the characteristic relaxation time  $\tau_p^{\text{eff}}$  in PEO/PMMA blends deviates from that of pure PEO (dashed black line) across all blend compositions and for all mode numbers beyond the monomer scale ( $N/p > 1$ ). Pure PEO approximately follows the expected Rouse scaling,  $\tau_p \sim p^{-2}$ ,<sup>74</sup> when using  $\tau_p^{\text{eff}}$ , which reflects stretched rather than single-exponential relaxation. As the mode number increases ( $p \rightarrow N$ ),  $\tau_p^{\text{eff}}$  for all blends converge, suggesting that relaxation behavior at the monomer scale, for PEO, is largely unaffected by the surrounding melt environment. In contrast, deviations from pure PEO behavior become more pronounced at lower  $p$  as the blend becomes more PMMA-rich

(decreasing  $x^{(\text{PEO})}$ ), indicating altered relaxation at longer length scales.

Figure 4B shows that the relaxation dynamics of PMMA chain segments, across all values of  $N/p$ , increasingly resemble those of PEO as  $x^{(\text{PEO})}$  increases. A notable distinction between PMMA and PEO is the non-monotonic behavior of  $\tau_p^{\text{eff}}$  for PMMA. Relaxation times begin to increase around  $N/p = 2$ , likely reflecting the dominance of local PMMA environments at short sub-chain lengths. This results in a nearly composition-independent enhancement of dynamics at short length scales, followed by growing deviations from neat PMMA behavior at longer scales. In contrast to PEO, where sufficiently short sub-chains recover the relaxation behavior of neat PEO, short PMMA sub-chains in blends never fully recover neat PMMA behavior. This highlights the persistent and composition-wide influence of PEO on PMMA dynamics, with the effect becoming more pronounced at larger length scales. The enhancement of PMMA dynamics due to PEO is also much stronger than the suppression of PEO dynamics due to PMMA.

Figure 4C shows that the enhanced deviation of PEO relaxation from the neat-polymer dynamics is accompanied by stronger departures from ideal Rouse-like behavior. Specifically, the stretching exponent  $\beta_p$  quantifies the extent to which the  $p$ th mode resembles ideal Rouse dynamics, for which  $\beta_p = 1$ . As  $x^{(\text{PEO})}$  decreases,  $\beta_p$  decreases across all modes, indicating increasingly non-ideal relaxation behavior across all segment length scales. Additionally, for a given blend composition, relaxation behavior becomes increasingly non-ideal at shorter length scales (lower  $N/p$ ). Conversely,  $\beta_p$  appears to plateau for  $N/p \geq 7$  and decrease for  $N/p < 7$ , except for neat PEO, which only exhibits a decrease in  $\beta_p$  for  $N/p < 2$ . In addition, in the  $N/p < 7$  regime, the degree of deviation strongly depends on blend composition. Together, these results suggest that dynamical coupling of the blend environment emerges at length scales of around 7 monomers of PEO and reflect the sensitivity of collective relaxation to compositional heterogeneity.

Analysis of the stretching coefficients for PMMA in Figure 4D further highlight PEO as

the dynamically dominant component in the blend on longer time scales ( $\geq 2000$  ps). While neat PMMA is strongly non-ideal in terms of its relaxation dynamics, the dynamics of PMMA in blends become more Rouse-like with increasing PEO content. Like PEO, PMMA exhibits enhanced deviation from ideality at shorter segment lengths; however, the onset of this deviation is composition-dependent for PMMA. In PEO-rich blends, the transition to enhanced non-ideality for PMMA begins around sub-chains of five monomers, which is comparable to the seven-monomer threshold observed for PEO in blends (Figure 4C). Conversely in PMMA-rich systems,  $\beta_p$  decreases for sub-chains of about two monomers. Although these conclusions are derived from results at 500 K, they extend to systems in the melt state at 360 K, as shown in the Supplementary Information, Figure S6.

### 3.5 Interplay Between Local Mobility and Relaxation Timescales

At this stage, we remark on an apparent contradiction between the results shown in Figures 4A and B and those in Figures 3C and 3F. Figure 3 indicates that PEO segmental mobility is suppressed even in the presence of a small number of nearby PMMA segments, whereas PMMA mobility is only notably affected when the local environment becomes significantly enriched in PEO ( $\tilde{\phi}_i^{(\text{PMMA})} < 0.5$ ). In contrast, the Rouse mode analysis suggests a stronger overall influence of PEO on PMMA than the reverse. In addition, the relaxation times for PMMA do not converge to the neat reference value, even for short sub-chains (high  $p$ ), whereas PEO dynamics do recover in similar limits.

Two factors help reconcile this discrepancy. First, although PEO appears more affected in absolute terms in Figure 3, normalizing by the neat-polymer reference reveals that PMMA experiences a much larger relative enhancement in dynamics in PEO-rich environments, as shown in the Supplementary Information, Figure S3. Second, there is also a fundamental distinction between the two measured quantities. Figure 3 relates to a segmental mobility, based on short-time fluctuations over a 100 ps interval, and Figure 4

relates to segmental relaxation, which reflects structural decorrelation, which occurs at much longer timescales. Thus, while local dynamics may appear similar over short times, this does not necessarily imply similar behavior in longer-time relaxation. We suspect that results between these analyses would begin to align if the time interval for assessing segmental mobility was substantially increased. This underscores a key nuance of dynamic heterogeneity, in that its effects depend on the timescale of the process being observed.

## 4 Conclusions

In this study, we systematically investigated blends of PEO and PMMA to uncover the molecular origins and consequences of dynamic heterogeneity at the nanoscale. Our study considered several facets, including the impact of overall blend composition, the influence of environmentally local composition, and the impact of temperature, assessing conditions above, between, and below the  $T_g$  of pure PEO and PMMA. We further quantified dynamic heterogeneity based on effects of local segmental mobility or fluctuations as well as larger-scale collective relaxation behaviors via Rouse mode analysis. The collection of simulations and analyses together provides a more comprehensive view relative to prior contributions that may have focused on a more limited set of compositions or temperatures.

Differences in local structure were deduced to asymmetrically impact local segmental mobilities. In particular, when accounting for differences in  $T_g$ , PEO segmental dynamics were enhanced relative to neat PEO, whereas the segmental dynamics of PMMA in blends were overall similar to  $T_g$ -equivalent neat PMMA systems. This disparity was elucidated by free-volume effects, where PEO segmental fluctuations correlated well with increases in local free volume, while PMMA dynamics were less impacted by reductions in free volume. Changes in the local environment also led to asymmetric effects on local segmental mobilities at short times. In terms of absolute magnitudes, suppression of fluctuations due

to a “slow” local environment was a stronger effect than enhancements by a “fast” local environment. However, relative to a neat-melt reference, the presence of PEO enhanced PMMA dynamics far more than PMMA suppressed those of PEO.

Rouse mode analysis for systems in the melt state further clarified the effects of compositional heterogeneity. Notably, PEO relaxation behavior approached that of the neat polymer in environments dominated by PEO (e.g., either sufficiently short length scales or in PEO-rich blends). In contrast, PMMA dynamics were consistently influenced by the presence of PEO, with PMMA segments in PEO-rich blends exhibiting PEO-like relaxation behavior except at the shortest length scales. Finally, the enhancement of PMMA relaxation dynamics in PEO-rich blends was substantially greater than the suppression of PEO dynamics in PMMA-rich blends, at least in the melt state. Together, these findings emphasize a directional coupling, wherein PMMA dominates the behavior of the blend at short timescales (100 ps) while PEO dynamics dominate at longer timescales ( $\geq 2000$  ps).

These findings extend our molecular-level understanding of how blending dynamically dissimilar polymers alters both local and collective segmental motions. The observation that PEO dynamics recover under certain conditions, while PMMA dynamics remain broadly perturbed, highlights a fundamental asymmetry in dynamical influence. Whether these behaviors generalize to other polymer blends with disparate relaxation properties or other thermal conditions remains an open question. Future work may examine the transferability of these packing-structure-dependent effects to other systems and examine their implications for macroscopic properties.<sup>10,75</sup> In addition, our results suggest that one species may have a stronger influence on dynamics at short times, while another may dominate at longer times, and the influence of a species may be apparent only at certain degrees of local composition. This perspective may offer a strategy to tune certain properties (e.g., viscoelastic properties or diffusion rates of other components, like ions or penetrants) across multiple length scales by adjusting the content and morphology of

dynamically distinct components.

## Acknowledgments

This research was supported by the National Science Foundation under Grant No. 2237470. S.Z. acknowledges additional support by Grant No. 2022398 from the United States-Israel Binational Science Foundation (BSF). Calculations were performed using resources from Princeton Research Computing at Princeton University, which is a consortium led by the Princeton Institute for Computational Science and Engineering (PICSciE) and Office of Information Technology's Research Computing.

## Data availability

The data underlying this study are available in the published article and its Supporting Information.

## Supporting Information

Calculation of apparent  $T_g$ ; calculation of free volume; influence of local environment on normalized segmental mobility; and Rouse mode analysis.

## References

- (1) Colby, R. H. Breakdown of time-temperature superposition in miscible polymer blends. *Polymer* **1989**, *30*, 1275–1278.
- (2) Roland, C. M.; Ngai, K. L. Dynamical heterogeneity in a miscible polymer blend. *Macromolecules* **1991**, *24*, 2261–2265, Publisher: American Chemical Society.

- (3) Kamath, S.; Colby, R. H.; Kumar, S. K. Dynamic Heterogeneity in Miscible Polymer Blends with Stiffness Disparity: Computer Simulations Using the Bond Fluctuation Model. *Macromolecules* **2003**, *36*, 8567–8573, Publisher: American Chemical Society.
- (4) Roland, C. M.; McGrath, K. J.; Casalini, R. Dynamic Heterogeneity in Poly(vinyl methyl ether)/Poly(2-chlorostyrene) Blends. *Macromolecules* **2006**, *39*, 3581–3587.
- (5) Sharma, R. P.; Green, P. F. Component Dynamics in Polymer/Polymer Blends: Role of Spatial Compositional Heterogeneity. *Macromolecules* **2017**, *50*, 6617–6630.
- (6) Zhang, G.; Rocha, S.; Lu, G.; Yuan, H.; Uji-i, H.; Floudas, G. A.; Müllen, K.; Xiao, L.; Hofkens, J.; Debroye, E. Spatially and Temporally Resolved Heterogeneities in a Miscible Polymer Blend. *ACS Omega* **2020**, *5*, 23931–23939.
- (7) Bennemann, C.; Donati, C.; Baschnagel, J.; Glotzer, S. C. Growing range of correlated motion in a polymer melt on cooling towards the glass transition. *Nature* **1999**, *399*, 246–249.
- (8) Phan, A. D.; Schweizer, K. S. Elastically Collective Nonlinear Langevin Equation Theory of Glass-Forming Liquids: Transient Localization, Thermodynamic Mapping, and Cooperativity. *The Journal of Physical Chemistry B* **2018**, *122*, 8451–8461.
- (9) Baker, D. L.; Reynolds, M.; Masurel, R.; Olmsted, P. D.; Mattsson, J. Cooperative Intramolecular Dynamics Control the Chain-Length-Dependent Glass Transition in Polymers. *Physical Review X* **2022**, *12*, 021047.
- (10) Ghanekarade, A.; Simmons, D. S. Combined Mixing and Dynamical Origins of Tg Alterations Near Polymer–Polymer Interfaces. *Macromolecules* **2023**, *56*, 379–392.
- (11) Fredrickson, G. H. The theory of polymer dynamics. *Current Opinion in Solid State & Materials Science* **1996**, *1*, 812–816.

- (12) Semenov, A. N.; Joanny, J.-F.; Khokhlov, A. R. Associating polymers: Equilibrium and linear viscoelasticity. *Macromolecules* **1995**, *28*, 1066–1075, Publisher: American Chemical Society.
- (13) Tanaka, K.; Takahara, A.; Kajiyama, T. Rheological Analysis of Surface Relaxation Process of Monodisperse Polystyrene Films. *Macromolecules* **2000**, *33*, 7588–7593, Publisher: American Chemical Society.
- (14) Mogurampelly, S.; Sethuraman, V.; Pryamitsyn, V.; Ganesan, V. Influence of nanoparticle-ion and nanoparticle-polymer interactions on ion transport and viscoelastic properties of polymer electrolytes. *The Journal of Chemical Physics* **2016**, *144*, 154905.
- (15) Zhang, A.; Moore, A. R.; Zhao, H.; Govind, S.; Wolf, S. E.; Jin, Y.; Walsh, P. J.; Riggleman, R. A.; Fakhraai, Z. The role of intramolecular relaxations on the structure and stability of vapor-deposited glasses. *The Journal of Chemical Physics* **2022**, *156*, 244703.
- (16) Fenton, D. E.; Parker, J. M.; Wright, P. V. Complexes of alkali metal ions with poly(ethylene oxide). *Polymer* **1973**, *14*, 589.
- (17) Berthier, C.; Gorecki, W.; Minier, M.; Armand, M. B.; Chabagno, J. M.; Rigaud, P. Microscopic investigation of ionic conductivity in alkali metal salts-poly(ethylene oxide) adducts. *Solid State Ionics* **1983**, *11*, 91–95.
- (18) Borodin, O.; Smith, G. D. Mechanism of Ion Transport in Amorphous Poly(ethylene oxide)/LiTFSI from Molecular Dynamics Simulations. *Macromolecules* **2006**, *39*, 1620–1629.
- (19) Webb, M. A.; Yamamoto, U.; Savoie, B. M.; Wang, Z.-G.; Miller, T. F. I. Globally Suppressed Dynamics in Ion-Doped Polymers. *ACS Macro Letters* **2018**, *7*, 734–738.

- (20) Chu, W.; Webb, M. A.; Deng, C.; Colón, Y. J.; Kambe, Y.; Krishnan, S.; Nealey, P. F.; de Pablo, J. J. Understanding Ion Mobility in P2VP/NMP<sup>+</sup>I<sup>-</sup> Polymer Electrolytes: A Combined Simulation and Experimental Study. *Macromolecules* **2020**, *53*, 2783–2792.
- (21) Deng, C.; Webb, M. A.; Bennington, P.; Sharon, D.; Nealey, P. F.; Patel, S. N.; de Pablo, J. J. Role of Molecular Architecture on Ion Transport in Ethylene oxide-Based Polymer Electrolytes. *Macromolecules* **2021**, *54*, 2266–2276.
- (22) Mu, D.; Huang, X.-R.; Lu, Z.-Y.; Sun, C.-C. Computer simulation study on the compatibility of poly(ethylene oxide)/poly(methyl methacrylate) blends. *Chemical Physics* **2008**, *348*, 122–129.
- (23) Schantz, S. Structure and Mobility in Poly(ethylene oxide)/Poly(methyl methacrylate) Blends Investigated by <sup>13</sup>C Solid-State NMR. *Macromolecules* **1997**, *30*, 1419–1425.
- (24) Lartigue, C.; Guillermo, A.; Cohen-Addad, J. P. Proton NMR investigation of the local dynamics in PEO/PMMA blends. *Journal of Polymer Science Part B: Polymer Physics* **1997**, *35*, 1059–1105.
- (25) Silva, G. G.; Machado, J. C.; Song, M.; Hourston, D. J. Nanoheterogeneities in PEO/PMMA blends: A modulated differential scanning calorimetry approach. *Journal of Applied Polymer Science* **2000**, *77*, 2034–2043, [\\_eprint: https://onlinelibrary.wiley.com/doi/pdf/10.1002/1097-4628\(20000829\)77:3A9%3C2034::AID-APP20%3E3.0.CO%3B2-Q](https://onlinelibrary.wiley.com/doi/pdf/10.1002/1097-4628(20000829)77:3A9%3C2034::AID-APP20%3E3.0.CO%3B2-Q).
- (26) Lutz, T. R.; He, Y.; Ediger, M. D.; Cao, H.; Lin, G.; Jones, A. A. Rapid Poly(ethylene oxide) Segmental Dynamics in Blends with Poly(methyl methacrylate). *Macromolecules* **2003**, *36*, 1724–1730.

- (27) Ghelichi, M.; Qazvini, N. T.; Jafari, S. H.; Khonakdar, H. A.; Farajollahi, Y.; Scheffler, C. Conformational, thermal, and ionic conductivity behavior of PEO in PEO/PMMA miscible blend: Investigating the effect of lithium salt. *Journal of Applied Polymer Science* **2013**, *129*, 1868–1874.
- (28) Choudhary, S. Effects of amorphous silica nanoparticles and polymer blend compositions on the structural, thermal and dielectric properties of PEO–PMMA blend based polymer nanocomposites. *Journal of Polymer Research* **2018**, *25*, 116.
- (29) Lim, Y. S.; Jung, H.-A.; Hwang, H. Fabrication of PEO-PMMA-LiClO<sub>4</sub>-Based Solid Polymer Electrolytes Containing Silica Aerogel Particles for All-Solid-State Lithium Batteries. *Energies* **2018**, *11*, 2559.
- (30) Sharon, D.; Deng, C.; Bennington, P.; Webb, M. A.; Patel, S. N.; de Pablo, J. J.; Nealey, P. F. Critical Percolation Threshold for Solvation-Site Connectivity in Polymer Electrolyte Mixtures. *Macromolecules* **2022**, *55*, 7212–7221.
- (31) Bakar, R.; Darvishi, S.; Li, T.; Han, M.; Aydemir, U.; Nizamoglu, S.; Hong, K.; Senses, E. Effect of Polymer Topology on Microstructure, Segmental Dynamics, and Ionic Conductivity in PEO/PMMA-Based Solid Polymer Electrolytes. *ACS Appl. Polym. Mater.* **2022**, *4*, 179–190.
- (32) Diddens, D.; Heuer, A.; Borodin, O. Understanding the Lithium Transport within a Rouse-Based Model for a PEO/LiTFSI Polymer Electrolyte. *Macromolecules* **2010**, *43*, 2028–2036.
- (33) Deng, C.; Webb, M. A.; Bennington, P.; Sharon, D.; Nealey, P. F.; Patel, S. N.; de Pablo, J. J. Role of Molecular Architecture on Ion Transport in Ethylene oxide-Based Polymer Electrolytes. *Macromolecules* **2021**, *54*, 2266–2276.

- (34) Webb, M. A.; Savoie, B. M.; Wang, Z.-G.; Miller III, T. F. Chemically Specific Dynamic Bond Percolation Model for Ion Transport in Polymer Electrolytes. *Macromolecules* **2015**, *48*, 7346–7358.
- (35) Niedzwiedz, K.; Wischniewski, A.; Monkenbusch, M.; Richter, D.; Genix, A.-C.; Arbe, A.; Colmenero, J.; Strauch, M.; Straube, E. Polymer Chain Dynamics in a Random Environment: Heterogeneous Mobilities. *Physical Review Letters* **2007**, *98*, 168301.
- (36) García Sakai, V.; Maranas, J. K.; Peral, I.; Copley, J. R. D. Dynamics of PEO in Blends with PMMA: Study of the Effects of Blend Composition via Quasi-Elastic Neutron Scattering. *Macromolecules* **2008**, *41*, 3701–3710, Publisher: American Chemical Society.
- (37) Brodeck, M.; Alvarez, F.; Moreno, A. J.; Colmenero, J.; Richter, D. Chain Motion in Nonentangled Dynamically Asymmetric Polymer Blends: Comparison between Atomistic Simulations of PEO/PMMA and a Generic Bead–Spring Model. *Macromolecules* **2010**, *43*, 3036–3051.
- (38) Sakai, V. G.; Chen, C.; Maranas, J. K.; Chowdhuri, Z. Effect of Blending with Poly(ethylene oxide) on the Dynamics of Poly(methyl methacrylate): A Quasi-Elastic Neutron Scattering Approach. *Macromolecules* **2004**, *37*, 9975–9983.
- (39) Liu, J.; Sakai, V. G.; Maranas, J. K. Composition Dependence of Segmental Dynamics of Poly(methyl methacrylate) in Miscible Blends with Poly(ethylene oxide). *Macromolecules* **2006**, *39*, 2866–2874.
- (40) Maranas, J. K. The effect of environment on local dynamics of macromolecules. *Current Opinion in Colloid & Interface Science* **2007**, *12*, 29–42.

- (41) Genix, A.-C.; Arbe, A.; Alvarez, F.; Colmenero, J.; Willner, L.; Richter, D. Dynamics of poly(ethylene oxide) in a blend with poly(methyl methacrylate): A quasielastic neutron scattering and molecular dynamics simulations study. *Physical Review E* **2005**, *72*, 031808.
- (42) Sakai, V. G.; Maranas, J. K.; Chowdhuri, Z.; Peral, I.; Copley, J. R. D. Miscible blend dynamics and the length scale of local compositions. *Journal of Polymer Science Part B: Polymer Physics* **2005**, *43*, 2914–2923.
- (43) Farago, B.; Chen, C.; Maranas, J. K.; Kamath, S.; Colby, R. H.; Pasquale, A. J.; Long, T. E. Collective motion in Poly(ethylene oxide)/poly(methylmethacrylate) blends. *Physical Review E* **2005**, *72*, 031809, Publisher: American Physical Society.
- (44) Zawada, J. A.; Ylitalo, C. M.; Fuller, G. G.; Colby, R. H.; Long, T. E. Component relaxation dynamics in a miscible polymer blend: poly(ethylene oxide)/poly(methyl methacrylate). *Macromolecules* **1992**, *25*, 2896–2902.
- (45) He, Y.; Lutz, T. R.; Ediger, M. D. Segmental and terminal dynamics in miscible polymer mixtures: Tests of the Lodge–McLeish model. *The Journal of Chemical Physics* **2003**, *119*, 9956–9965.
- (46) Dudowicz, J.; Freed, K. F.; Douglas, J. F. Concentration fluctuations in miscible polymer blends: Influence of temperature and chain rigidity. *The Journal of Chemical Physics* **2014**, *140*, 194901.
- (47) Dudowicz, J.; Douglas, J. F.; Freed, K. F. Two glass transitions in miscible polymer blends? *The Journal of Chemical Physics* **2014**, *140*, 244905.
- (48) Moreno, A. J.; Colmenero, J. Tests of mode coupling theory in a simple model for two-component miscible polymer blends. *Journal of Physics: Condensed Matter* **2007**, *19*, 466112.

- (49) Ngai, K. L.; Wang, L.-M. Interchain coupled chain dynamics of poly(ethylene oxide) in blends with poly(methyl methacrylate): Coupling model analysis. *The Journal of Chemical Physics* **2011**, *135*, 194902.
- (50) Ngai, K. L.; Capaccioli, S. Unified explanation of the anomalous dynamic properties of highly asymmetric polymer blends. *The Journal of Chemical Physics* **2013**, *138*, 054903.
- (51) Colmenero, J. Comment on “Unified explanation of the anomalous dynamic properties of highly asymmetric polymer blends” [J. Chem. Phys. 138, 054903 (2013)]. *The Journal of Chemical Physics* **2013**, *138*, 197101.
- (52) Ngai, K. L.; Capaccioli, S. Response to “Comment on ‘Unified explanation of the anomalous dynamic properties of highly asymmetric polymer blends’” [J. Chem. Phys. 138, 197101 (2013)]. *The Journal of Chemical Physics* **2013**, *138*, 197102.
- (53) Colmenero, J. A Generalized Rouse Incoherent Scattering Function for Chain Dynamics of Unentangled Polymers in Dynamically Asymmetric Blends. *Macromolecules* **2013**, *46*, 5363–5370, Publisher: American Chemical Society.
- (54) Colmenero, J. Reply to “Comment on ‘A Generalized Rouse Incoherent Scattering Function for Chain Dynamics of Unentangled Polymers in Dynamically Asymmetric Blends’”. *Macromolecules* **2013**, *46*, 8056–8058, Publisher: American Chemical Society.
- (55) Ngai, K. L.; Capaccioli, S. Comment on “A Generalized Rouse Incoherent Scattering Function for Chain Dynamics of Unentangled Polymers in Dynamically Asymmetric Blends”. *Macromolecules* **2013**, *46*, 8054–8055, Publisher: American Chemical Society.

- (56) Chen, C.; Maranas, J. K. A Molecular View of Dynamic Responses When Mixing Poly(ethylene oxide) and Poly(methyl methacrylate). *Macromolecules* **2009**, *42*, 2795–2805, Publisher: American Chemical Society.
- (57) Brodeck, M.; Alvarez, F.; Colmenero, J.; Richter, D. Single Chain Dynamic Structure Factor of Poly(ethylene oxide) in Dynamically Asymmetric Blends with Poly(methyl methacrylate). Neutron Scattering and Molecular Dynamics Simulations. *Macromolecules* **2012**, *45*, 536–542, Publisher: American Chemical Society.
- (58) Thompson, A. P.; Aktulga, H. M.; Berger, R.; Bolintineanu, D. S.; Brown, W. M.; Crozier, P. S.; in't Veld, J. J.; Kohlmeyer, A.; Moore, S. G.; Nguyen, T. D.; Shan, R.; Stevens, M. J.; Tranchida, J.; Trott, C.; Plimpton, S. J. LAMMPS - a flexible simulation tool for particle-based materials modeling at the atomic, meso, and continuum scales. *Computer Physics Communications* **2022**, *271*, 108171.
- (59) William L. Jorgensen, D. S. M.; Tirado-Rives, J. Development and Testing of the OPLS All-Atom Force Field on Conformational Energetics and Properties of Organic Liquids. *Journal of the American Chemical Society* **1996**, *118*, 11225–11236.
- (60) Hockney, R. W.; Eastwood, J. W. *Computer simulation using particles*; 1988.
- (61) Pollock, E. L.; Glosli, J. Comments on P3M, FMM, and the Ewald method for large periodic Coulombic systems. *Computer Physics Communications* **1996**, *95*, 93–110.
- (62) Hanwell, M. D.; Curtis, D. E.; Lonie, D. C.; Vandermeersch, T.; Zurek, E.; Hutchinson, G. R. Avogadro: An advanced semantic chemical editor, visualization, and analysis platform. *Journal of Cheminformatics* **2012**, *4*, 17.
- (63) Avogadro: an open-source molecular builder and visualization tool. Version 1.2.0. <http://avogadro.cc/>.

- (64) Hiemenz, P. C.; Lodge, T. *Polymer Chemistry*, 2nd ed.; CRC Press, 2007.
- (65) Buchholz, J.; Paul, W.; Varnik, F.; Binder, K. Cooling rate dependence of the glass transition temperature of polymer melts: Molecular dynamics study. *The Journal of Chemical Physics* **2002**, *117*, 7364–7372.
- (66) Han, J.; Gee, R. H.; Boyd, R. H. Glass Transition Temperatures of Polymers from Molecular Dynamics Simulations. *Macromolecules* **1994**, *27*, 7781–7784.
- (67) Rigby, D.; Roe, R. J. Molecular dynamics simulation of polymer liquid and glass. 4. Free-volume distribution. *Macromolecules* **1990**, *23*, 5312–5319.
- (68) Putta, S.; Nemat-Nasser, S. Molecularly-based numerical evaluation of free volume in amorphous polymers. *Materials Science and Engineering: A* **2001**, *317*, 70–76.
- (69) Widmer-Cooper, A.; Harrowell, P. Free volume cannot explain the spatial heterogeneity of Debye–Waller factors in a glass-forming binary alloy. *Journal of Non-Crystalline Solids* **2006**, *352*, 5098–5102.
- (70) Mei, B.; Zhuang, B.; Lu, Y.; An, L.; Wang, Z.-G. Local-Average Free Volume Correlates with Dynamics in Glass Formers. *The Journal of Physical Chemistry Letters* **2022**, *13*, 3957–3964, Publisher: American Chemical Society.
- (71) Wu, S. Entanglement, friction, and free volume between dissimilar chains in compatible polymer blends. *Journal of Polymer Science Part B: Polymer Physics* **1987**, *25*, 2511–2529.
- (72) Moynihan, C. T.; Eastale, A. J.; Wilder, J.; Tucker, J. Dependence of the glass transition temperature on heating and cooling rate. *The Journal of Physical Chemistry* **1974**, *78*, 2673–2677.

- (73) Hung, J.-H.; Patra, T. K.; Simmons, D. S. Forecasting the experimental glass transition from short time relaxation data. *Journal of Non-Crystalline Solids* **2020**, *544*, 120205.
- (74) Brodeck, M.; Alvarez, F.; Arbe, A.; Juranyi, F.; Unruh, T.; Holderer, O.; Colmenero, J.; Richter, D. Study of the dynamics of poly(ethylene oxide) by combining molecular dynamic simulations and neutron scattering experiments. *The Journal of Chemical Physics* **2009**, *130*, 094908.
- (75) Ngai, K. L.; Valenti, S.; Capaccioli, S. Molecular dynamic in binary mixtures and polymer blends with large difference in glass transition temperatures of the two components: A critical review. *Journal of Non-Crystalline Solids* **2021**, *558*, 119573.

# Supporting Information

## Asymmetric Effects Underlying Dynamic Heterogeneity in Miscible Blends of Poly(methyl methacrylate) with Poly(ethylene oxide)

Shannon Zhang and Michael A. Webb\*

*Department of Chemical and Biological Engineering, Princeton University, Princeton, NJ  
08544, USA*

E-mail: mawebb@princeton.edu

### Contents

S1 Calculation of apparent $T_g$	SI-2
S2 Calculation of free-volume	SI-4
S3 Influence of local environment on normalized segmental mobility	SI-5
S4 Rouse mode analysis	SI-6

## S1 Calculation of apparent $T_g$

The simulated  $T_g$  is calculated using a bootstrapping process that is repeated 10,000 times. The start and end points of the high and low temperature regions selected for each bootstrapping process are given in Table S1. The simulated specific volume versus temperature data used in this calculation, final  $T_g$  values, and example linear regressions in the high and low temperature regions for all blends studied are given in Figure S1.

**Table S1:** Start and end points and ranges of temperature used to calculate linear regressions in the high and low temperature regions of specific volume versus temperature data for  $T_g$  calculations of PEO/PMMA blends.

Composition	Glassy region fit	Liquid region fit
100 PEO%	100-[150,250]	[300,400]-450
90 PEO%	100-[150,250]	[350,450]-500
80 PEO%	100-[150,250]	[350,450]-500
70 PEO%	100-[150,250]	[400,500]-550
60 PEO%	100-[150,250]	[400,500]-550
50 PEO%	150-[200,300]	[400,500]-550
40 PEO%	150-[200,300]	[400,500]-550
30 PEO%	150-[200,300]	[440-540]-590
20 PEO%	200-[250,350]	[440-540]-590
10 PEO%	200-[250,350]	[500,600]-650
0 PEO%	200-[250,350]	[500,600]-650

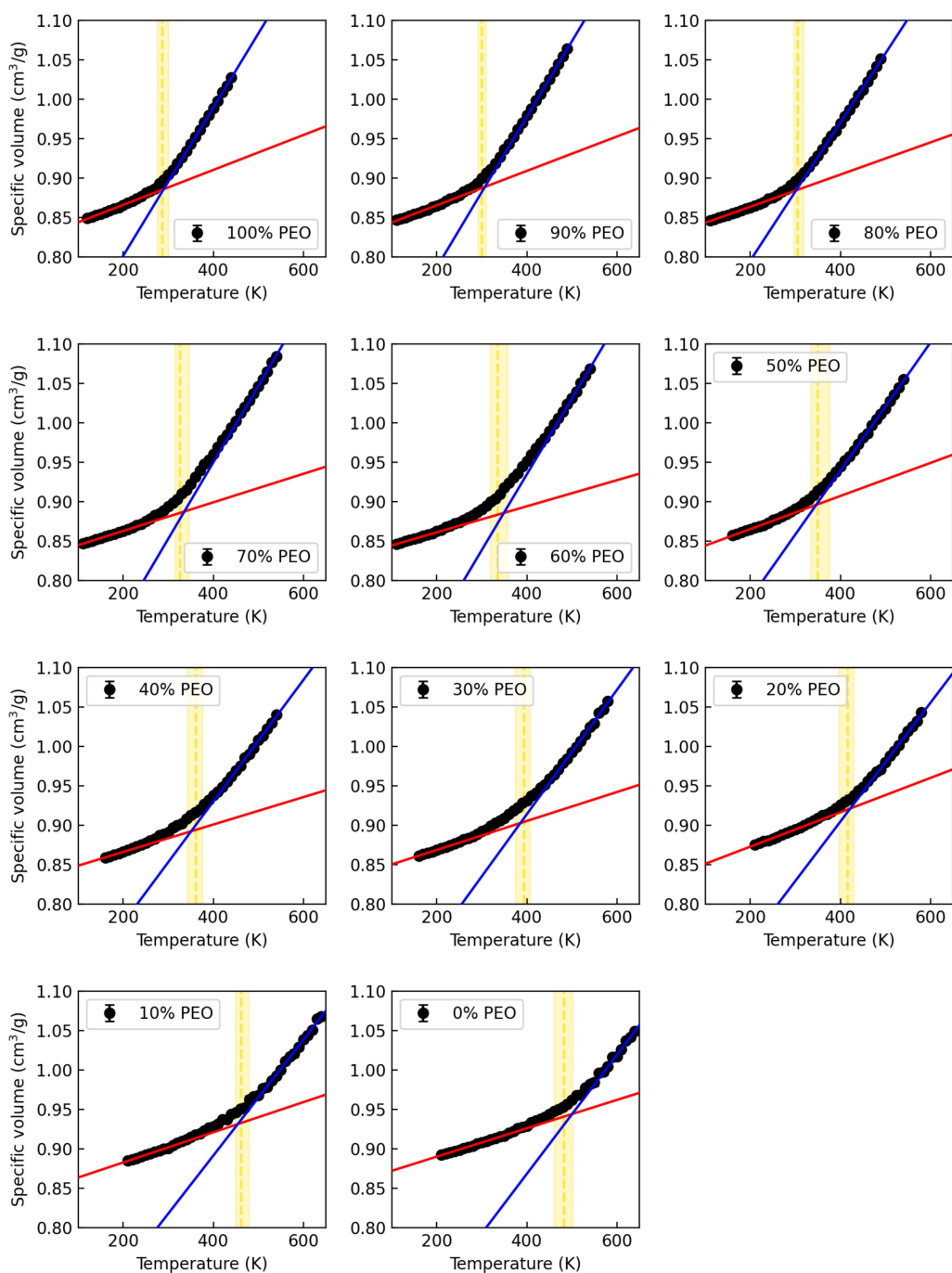


**Figure S1:** Change in specific volume with temperature used to calculate  $T_g$  for PEO/PMMA blends over blend composition. Each marker and error bar is an average and standard error, respectively, of the specific volume of three independent system configurations at a given temperature. The vertical dashed yellow line is the final calculated  $T_g$ . The shaded yellow region is the range of all  $T_g$  values calculated in the bootstrapping process. The red and blue lines are example linear regressions of one instance of the bootstrapping process for the high and low temperature regions, respectively.

## S2 Calculation of free-volume

The size of the probe used in the free volume calculation dictates the magnitude of free volume calculated for a polymer chain. Probes that are too large will underestimate free volume while probes that are too small will overestimate. However, we are interested in the qualitative change in free volume with  $x_{\text{PEO}}$ . To ensure that probe size does not affect our analysis, we calculated free volume using probes of radius 0.25 Å and 0.5 Å. These values are smaller than the size of the smallest atom in the polymer, hydrogen, which has a  $\sigma = 1.008$  Å. As shown in Figure S2, we observe that adjusting the probe size affects the magnitude of free volume surrounding the chain, as expected, but does not change the qualitative trends in free volume versus  $x_{\text{PEO}}$ . Thus, using any of these probe sizes would be adequate for the analysis presented in the main text. We proceed using probes of radius 0.5 Å.

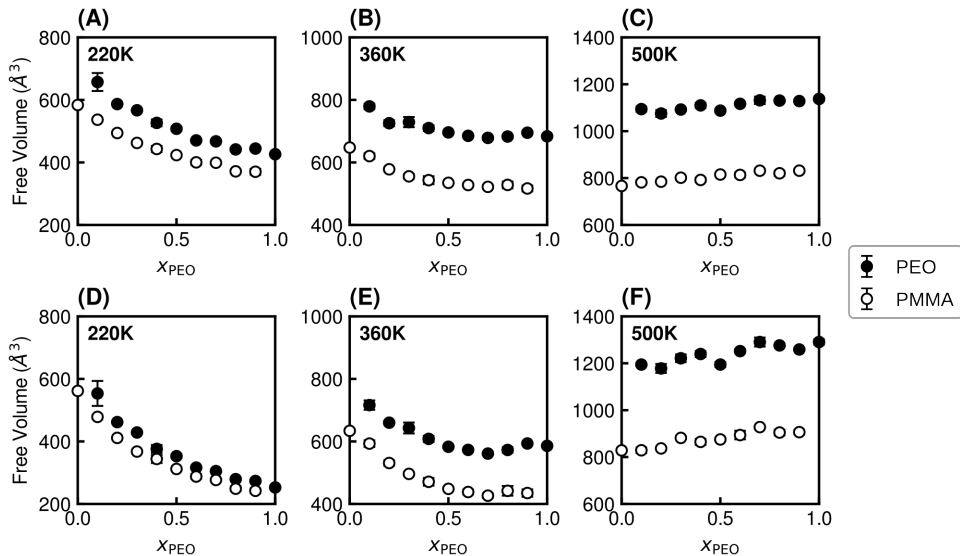


**Figure S2:** Local free volume of PEO and PMMA chains versus blend composition calculated using different probe radii. Free volume is calculated using probes of radius (A-C) 0.25 Å and (D-F) 0.5 Å. Error bars are standard errors calculated for three independent system configurations.

### S3 Influence of local environment on normalized segmental mobility

Analysis of the segmental mobility as a function of local mobility in Section 3.3 reveals that changes to the local environment lead to larger magnitudes of  $\mu_{i,\Delta t}$  suppression than  $\mu_{i,\Delta t}$  enhancement. However,  $\mu_{i,\Delta t}$  normalized by the local mobility of each neat species ( $\mu_{i,\Delta t}^{\circ}$ ), shown in Figure S3, reveals that the local environment actually has a much larger relative effect on the enhancement of normalized  $\mu_{i,\Delta t}$  than the suppression of normalized  $\mu_{i,\Delta t}$ .

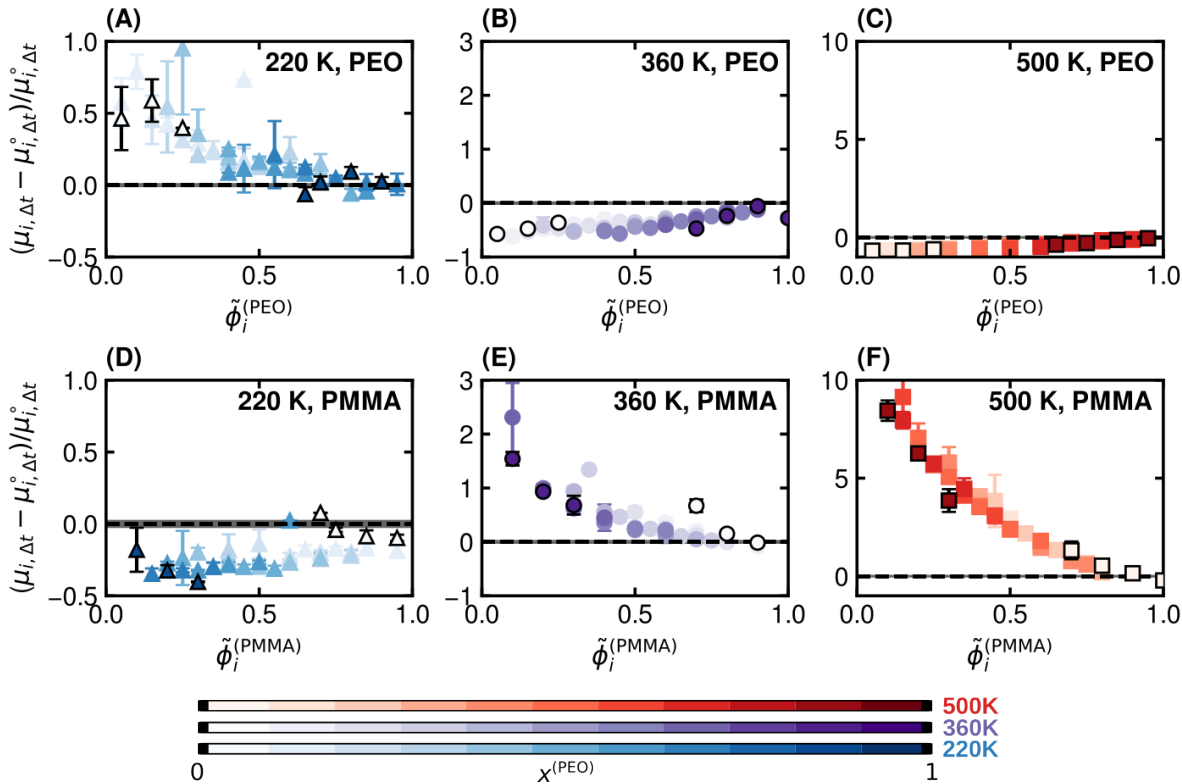


**Figure S3:** Variation in normalized relative segmental mobility over local environment. Results are shown for PEO at (A) 220 K, (B) 360 K, and (C) 500 K and PMMA at (D) 220 K, (E) 360 K, and (F) 500 K. Segmental mobility is calculated relative to and normalized by  $\mu_{i,\Delta t}$  of the neat polymers, denoted as  $\mu_{i,\Delta t}^{\circ}$ . The color gradient corresponds to a gradient in blend composition containing the most PEO (dark) to the least PEO (light). Results for chains in blends with the most extreme compositions ( $x^{(\text{PEO})} = 0.1$  and  $0.9$ ) are outlined in black as a visual aid. Error bars are standard errors for three independent system configurations at a given composition and temperature. Horizontal dashed lines correspond to the relative segmental mobility of (A-C) pure PEO and (D-F) pure PMMA. The gray area around the dashed lines are standard deviations calculated from three independent configurations of the neat systems.

## S4 Rouse mode analysis

Effective relaxation times and stretching parameters used in the Rouse mode analysis are extracted from normalized Rouse mode ACFs of PEO and PMMA. Representative ACFs from one run per  $x^{(\text{PEO})}$  at 500 K and their fits using values of  $\tau_p^{\text{eff}}$  and  $\beta_p$  calculated from the linear regression method described in Section 2.2.4 are shown for PEO and PMMA in Figures S4 and S5, respectively. Results from the Rouse mode analysis for systems at 360 K that are in a melt state are shown in Figure S6. Results are restricted to systems with  $x^{(\text{PEO})} \geq 0.6$ , as 360 K is greater than the blend  $T_g$  of these systems, reflecting their apparent melt state.

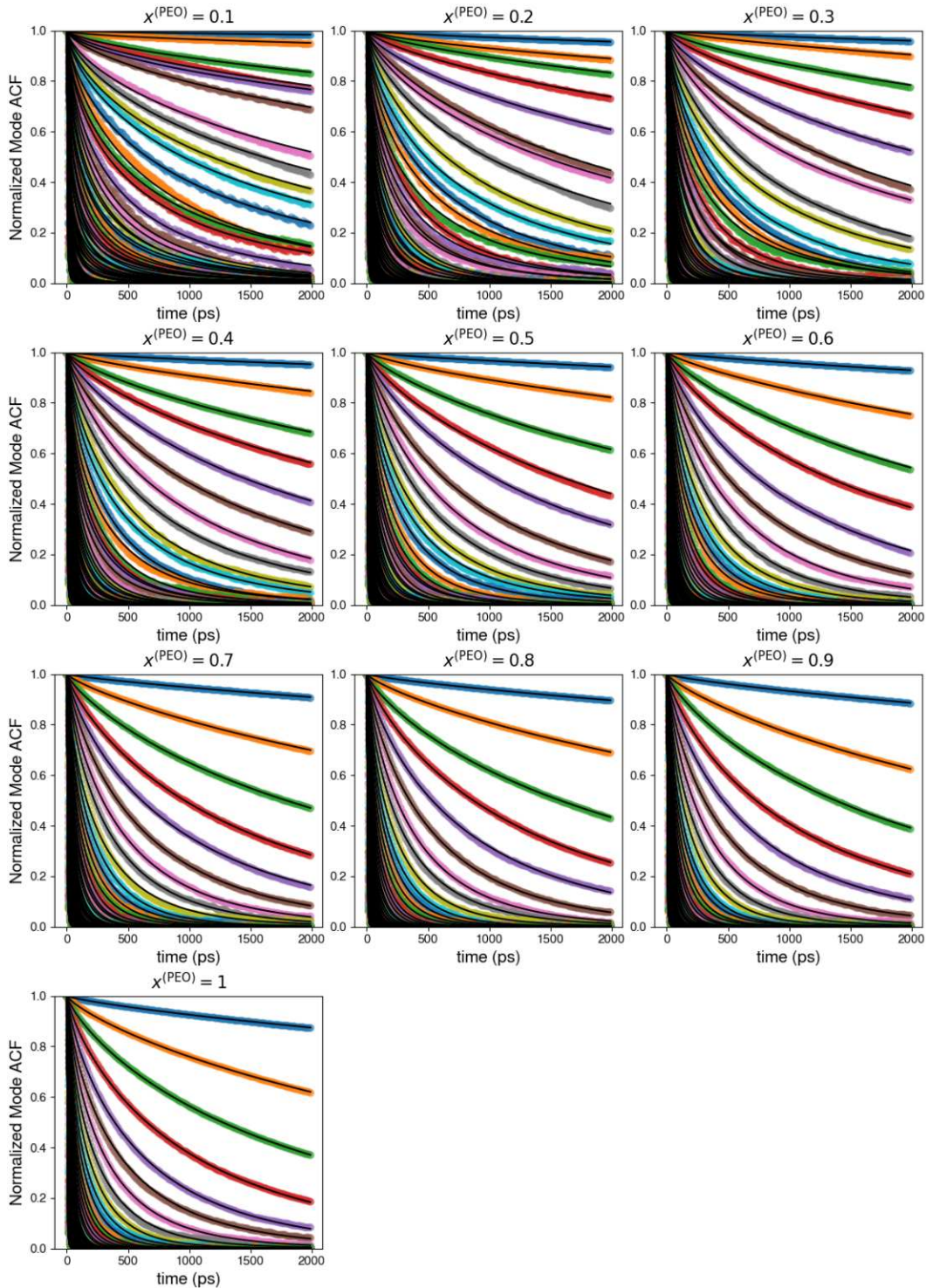


**Figure S4:** Normalized Rouse mode autocorrelation functions (ACFs) and their fits for PEO chains in the first run of each blend composition. Each ACF shown in each panel is for one Rouse mode. The topmost ACF is the ACF for the  $p = 0$ th Rouse mode, the ACF below it is for the  $p = 1$ st Rouse mode, and so on. The ACFs of all 74 Rouse modes for PEO are plotted. Black solid lines are fits to each ACF.

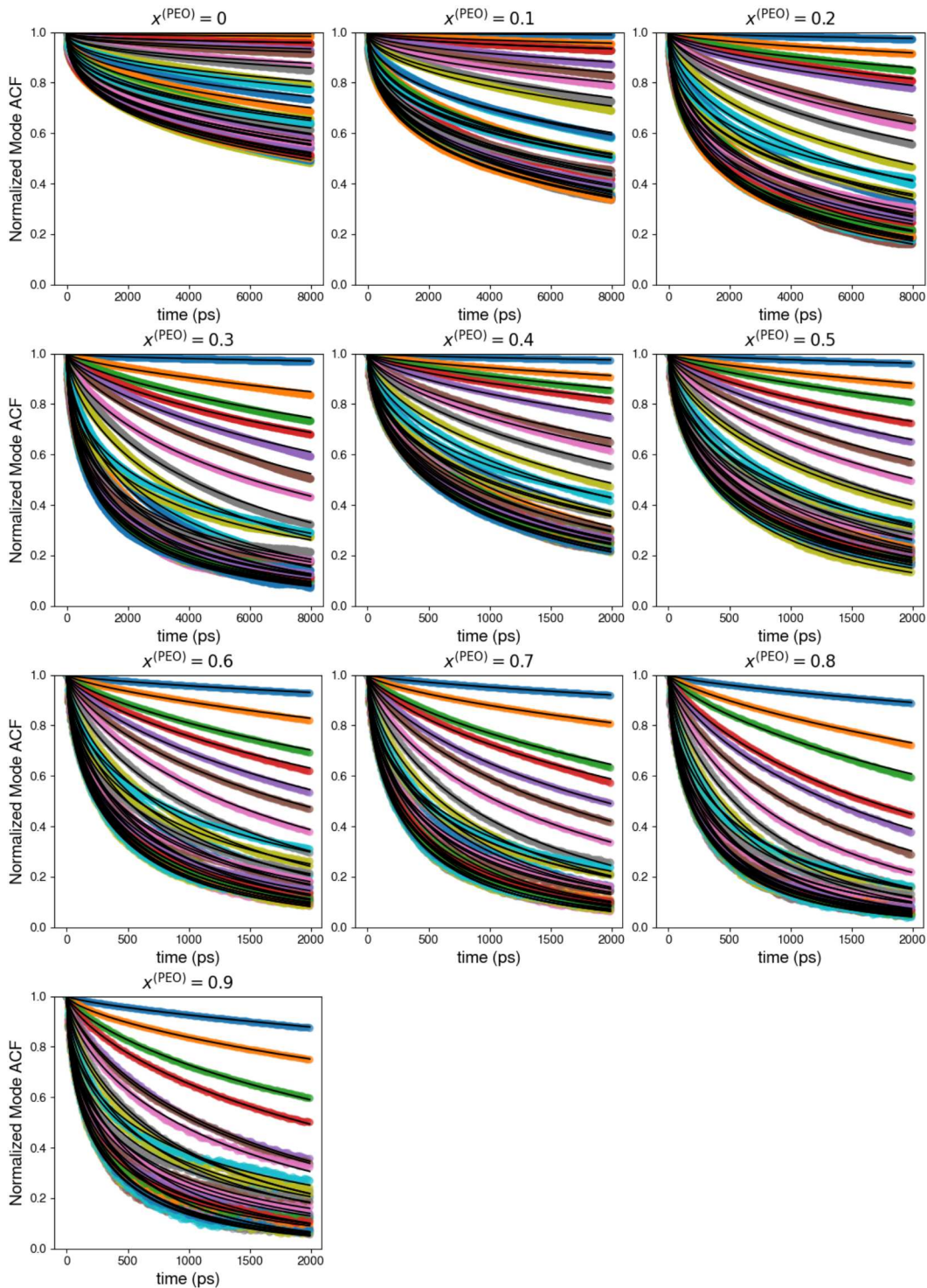


**Figure S5:** Normalized Rouse mode autocorrelation functions (ACFs) and their fits for PMMA chains in the first run of each blend composition. Each ACF shown in each panel is for one Rouse mode. The topmost ACF is the ACF for the  $p = 0$ th Rouse mode, the ACF below it is for the  $p = 1$ st Rouse mode, and so on. The ACFs of all 32 Rouse modes for PMMA are plotted. Black solid lines are fits to each ACF.

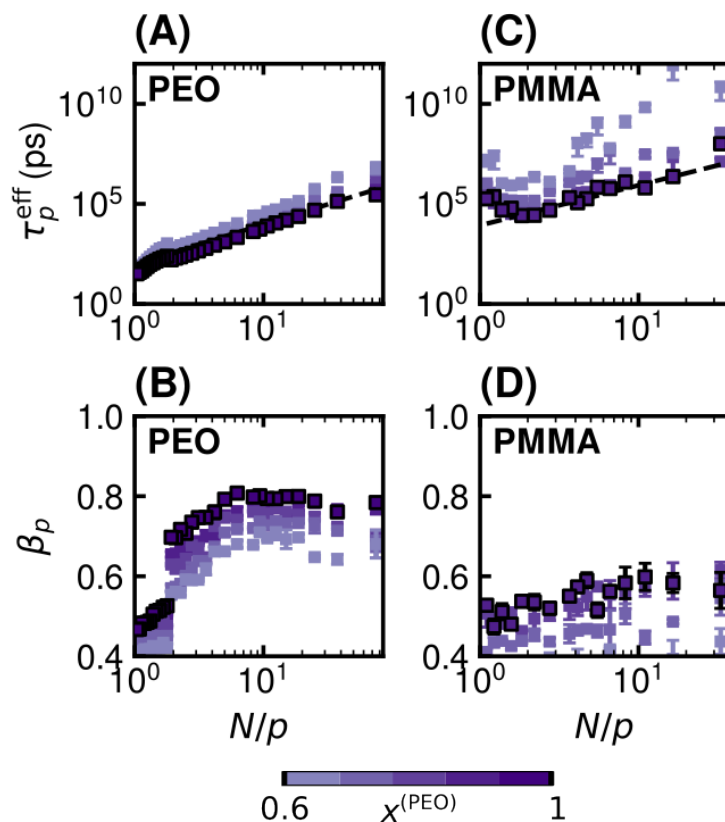


**Figure S6:** Variation in dynamics of PEO and PMMA with chain length and blend composition for chains in blends at 360 K. The (A,B) effective relaxation time  $\tau_p^{\text{eff}}$  and (C,D) stretching parameter  $\beta_p$  are plotted against  $N/p$ , where  $N$  is the number of monomers in a chain and  $p$  is the Rouse mode. For  $p > 8$ , data points are only shown for every third value of  $p$  to prevent overcrowding the data points on the figure for ease of visualization. Dashed black lines (A,B) indicate ideal Rouse mode number dependence. Results for chains in blends with the most PEO are outlined in black as a visual aid. Error bars are standard errors for three independent system configurations at a given composition.